(12)

FERROELECTRIC TUNGSTEN BRONZE BULK CRYSTALS AND EPITAXIAL THIN FILMS FOR ELECTRO-OPTIC DEVICE APPLICATIONS

Semi-Annual Technical Report No. 1
For Period 09/30/82 through 03/31/83

May 1983

DARPA Order No.	4540
Program Code:	P2D10
Name of Contractor:	Rockwell International Corporation
Effective Date of Contract:	9/30/82
Contract Expiration Date:	11/13/84
Amount of Contract Dollars:	$613,858
Contract Number:	N00014-82-C-2466
Principal Investigators:	Dr. R.R. Neurgaonkar (805) 498-4545, Ext. 109
	Dr. L.E. Cross Pennsylvania State University (814) 865-1181

Sponsored by

Defense Advanced Research Projects Agency (DoD)
DARPA Order No. 4540
Monitored by Naval Research Laboratory
Under Contract No. N00014-82-C-2466

The views and conclusions contained in this document are those of the authors and should not be interpreted as necessarily representing the official policies, either expressed or implied, of the Defense Advanced Research Projects Agency or the United States Government.

Approved for public release; distribution unlimited.

19 Landolt Börnstein, Ferroelectrics and Related Substances, New Seres, Vol. 16 (1981).

20. T.R. Shrout, Ferroelectrics Lett. 44, 325 (1983).

UNCLASSIFIED

SECURITY CLASSIFICATION OF THIS PAGE (When Data Entered)

REPORT DOCUMENTATION PAGE

READ INSTRUCTIONS BEFORE COMPLETING FORM

1. REPORT NUMBER

2. GOVT ACCESSION NO. A129351

3. RECIPIENT'S CATALOG NUMBER

4. TITLE (and Subtitle)
FERROELECTRIC TUNGSTEN BRONZE BULK CRYSTALS AND EPITAXIAL THIN FILMS FOR ELECTRO-OPTIC DEVICE APPLICATIONS

5. TYPE OF REPORT & PERIOD COVERED
Semi-Annual Tech Rpt #1 for period 09/30/82-03/31/83

6. PERFORMING ORG. REPORT NUMBER
SC5340.2SA

7. AUTHOR(s)
R.R. Neurgaonkar, L.E. Cross

8. CONTRACT OR GRANT NUMBER(s)
N00014-82-C-2466

9. PERFORMING ORGANIZATION NAME AND ADDRESS
Rockwell International Science Center
1C49 Camino Dos Rios
Thousand Oaks, CA 91360

10. PROGRAM ELEMENT, PROJECT, TASK AREA & WORK UNIT NUMBERS
DARPA No. 4540

11. CONTROLLING OFFICE NAME AND ADDRESS
Naval Research Laboratory
4555 Overlook Avenue S.W.
Washington, DC 20375

12. REPORT DATE
May 1983

13. NUMBER OF PAGES
51

14. MONITORING AGENCY NAME & ADDRESS(if different from Controlling Office)

15. SECURITY CLASS. (of this report)
Unclassified

15a. DECLASSIFICATION/DOWNGRADING SCHEDULE

16. DISTRIBUTION STATEMENT (of this Report)
Approved for public release; distribution unlimited.

17. DISTRIBUTION STATEMENT (of the abstract entered in Block 20, if different from Report)

18. SUPPLEMENTARY NOTES

19. KEY WORDS (Continue on reverse side if necessary and identify by block number)
SBN, PBN, Czochralski, LPE Growth. Tungsten Bronze, Flux Systems, Electro-optic Coefficients, Striations, Birefringence

20. ABSTRACT (Continue on reverse side if necessary and identify by block number)
3 cm diameter single crystals of the bronze compositions SBN:50 and SBN:60 have been successfully grown. Optical striations in SBN:60 are found to arise from impurities and temperature instability during growth. Improvements in temperature stability, rotation rate, and post-annealing conditions have improved the optical quality considerably.

LPE growth of SBN:48 on SBN:60 and SBN:50 single crystal substrates has been successful, with crystal films of 10 - 15 μm in thickness grown.

DD FORM 1 JAN 73 1473 EDITION OF 1 NOV 65 IS OBSOLETE

UNCLASSIFIED

SECURITY CLASSIFICATION OF THIS PAGE (When Data Entered)

Piezoelectric and electro-optic measurements have been performed on PBN and SBN single crystals. Electro-optic g and r coefficients are shown to be easily determined from measurement of the birefringence Δn_{31}. The linear r coefficients are particularly promising for both PBN and SBN.

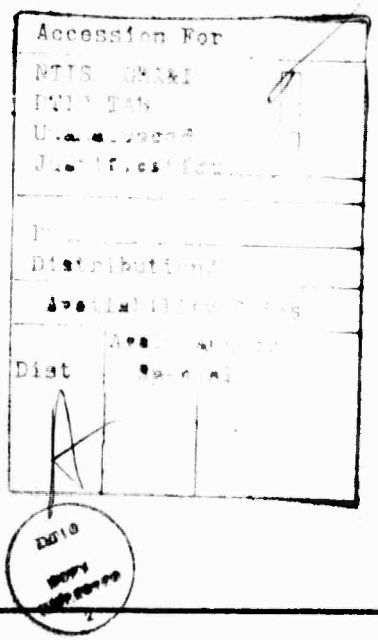

TABLE OF CONTENTS

LIST OF TABLES

LIST OF ILLUSTRATIONS

1.0 PROGRESS AND TECHNICAL SUMMARY

1.1 Purpose of Investigation

Over the past decade, there has been a dramatic upsurge of interest in electro-optic, acousto-optic and nonlinear-optical techniques driven by the needs in optical communications, optical switching, optical signal processing, spectrum analysis, direction of arrival (DOA) analysis and many other electronic warfare applications. The era has been characterized by the successful laboratory demonstration of many new interesting and attractive device concepts, a number of which are of high relevance to specific DoD needs. It has also, however, been singularly lacking in any significant advance in the available materials base for these demanding systems requirements.

A large number of ferroelectric crystals have been grown and characterized, and many of these have properties that are extremely attractive for optical applications. In particular, many of the ferroelectrics have high electro-optic, acousto-optic and nonlinear optical coefficients. However, only a few ferroelectrics, such as ammonium dyhydrogen phosphate and lithium niobate, have found wide application in the optics area. Other ferroelectric materials which exhibit much higher electro-optic coefficients, as well as favorable nonlinear characteristics, have not been exploited on a practical basis because of difficulties in growing large, striation-free single crystals.

The purpose of the present investigation is to develop tungsten bronze ferroelectric crystals that exhibit high electro-optic and nonlinear optical properties that are useful for device applications. The recent success at our laboratory in growing large crystals of SBN:60 and SBN:50 and many other materials could represent a major breakthrough in new materials development for potential optical device applications. Although some of these crystals exhibit striations and other optical defects, in general these tungsten bronze crystals have very high electro-optic and nonlinear optical coefficients. Hence, it is important that these materials be further exploited. The major goal of this investigation is, then, the development of suitable growth techniques by which crystal quality can be sufficiently improved for optical device applications.

1.2 Current Research Results

The tungsten bronze structural family offers a large number of crystals for electro-optic, nonlinear optical and many other applications; however, the current work has mainly focused on the development of optical quality crystals/films from the bronze $Sr_{1-x}Ba_xNb_2O_6$ (SBN) system. The composition $Sr_{0.6}Ba_{0.4}Nb_2O_6$ (SBN:60) has been reported to be the only congruent melting composition in the $SrNb_2O_6$-$BaNb_2O_6$ system, and this composition has also been found to be relatively easy to grow.

During the last six months, considerable progress has been made in several areas, including single crystal and thin film growth and characterization. The new Czochralski unit has now been installed and crystals of the bronze compositions SBN:60 and SBN:50 as large as 1 to 3 cm in diameter have been grown. Although SBN:60 single crystals appear to be reasonably good for optical studies, these crystals do exhibit striations. The results of this investigation indicate that the striations develop even when using higher purity materials because of a change in the Sr/Ba ratio resulting from temperature instability during growth. Over the last six months, considerable effort has been made to improve the temperature stability during growth and the post-annealing conditions after growth, and this has proven to be effective in reducing striations significantly, but not completely. This is, however, a promising result, and future work is aimed at improving the temperature stability still further, so that the quality of the crystals can be sufficiently enhanced for use in optical device applications.

Solvent selection and the experimental set-up for the liquid phase epitaxial (LPE) growth work for the bronze SBN system has been successfully established. Several systems, including BaV_2O_6-$Sr_{0.5}Ba_{0.5}Nb_2O_6$ and SrV_2O_6-$Sr_{0.5}Ba_{0.5}Nb_2O_6$, have been shown to be suitable for developing epilayers of SBN compositions; however, the present work has mainly concentrated on the BaV_2O_6-$Sr_{0.5}Ba_{0.5}Nb_2O_6$ system. SBN:60 and SBN:50 single crystal wafers have been used as substrate materials for this growth and the technique has been shown to be successful for the growth of approximately 10 - 15 μm thick films.

A number of piezoelectric and optical measurements have been performed on single crystal samples of SBN and PBN ($Pb_{1-x}Ba_xNb_2O_6$) bronze compositions. The electro-optic g (quadratic) coefficients were easily obtained by measurement of the birefringence Δn_{31}. These coefficients were found to be virtually temperature-independent and varied little with composition, in agreement with earlier theoretical work which showed that the g coefficients depend primarily on the oxygen framework and not on the cation make-up of the structure. Calculated values for the electro-optic r coefficients, however, strongly reflect the temperature dependence of the polarization P_s and the dielectric constants of the given bronze system. The values for $(r_{33} - r_{13})$ and r_{15} are very promising in both SBN and PBN, with r_{15} being particularly high for the near-morphotropic $Pb_{0.56}Ba_{0.44}Nb_2O_6$ composition.

2.0 DEVELOPMENT OF TUNGSTEN BRONZE MATERIALS

2.1 Materials Growth Techniques

Since most of the bronze compositions grown in our laboratory are based on solid solution systems, it is important that suitable growth techniques be developed to produce crystals free of optical defects such as striations, scattering centers and twinning. Striations and other defects are typical problems common to solid solution crystals and it is often difficult to suppress them completely; however, these problems can effectively be reduced such that the crystals can be useful for optical device studies. This task is difficult; hence, the selection of appropriate growth techniques is critical in the present work. At present, three different techniques have been chosen to develop SBN and other bronze crystals. They are as follows:

1. Bulk Single Crystals: Czochralski Technique
2. Thin Films: Liquid Phase Epitaxy (LPE)
3. Strip Crystals: Edge Defined Film-Fed Technique.

The first two techniques are well established in our current work, and bulk crystals and films of SBN compositions have already been grown. In the present report the growth of SBN crystals and films is discussed with the associated growth problems. The last proposed technique (strip crystals) which we intend to use in this work will be initiated in the latter part of this program.

2.2 Tungsten Bronze Family

The tungsten bronze compositions can be represented by the general formulae $(A_1)_4(A_2)_2C_4B_{10}O_{30}$ and $(A_1)_4(A_2)_2B_{10}O_{30}$, in which A_1, A_2, C and B are 15-, 12-, 9-, and 6-fold coordinated sites in the structures. In the first case all of the crystallographic sites are occupied, and hence the composition is referred to as a "filled" bronze structure. In the second case the crystallo-

graphic site C is vacant, hence it is referred to as an "unfilled" bronze structure. Based on these formulae, at least 150 known compounds and several solid solution systems exist in this family; hence there is a great possibility to develop suitable bronze compositions for electro-optic applications. As summarized in Table 1, this family can be further divided into two sub-groups according to unit cell dimensions, crystal growth habit, and physical properties including electro-optic, dielectric, electro-mechanical, etc. The compositions from each group exhibit interesting properties; however, the emphasis in the present work is on the smaller unit cell bronze compositions such as $Sr_{1-x}Ba_xNb_2O_6$, where x = 0.40 and 0.50. This group of materials is reasonably well characterized and offers an excellent opportunity for the development of optical-grade material.

2.3 Growth Problems Associated with the $Sr_{1-x}Ba_xNb_2O_6$ System Crystals

The single crystal growth of the ferroelectric composition $Sr_{1-x}Ba_xNb_2O_6$, where x = 0.40 and 0.50, has been studied for the last 3 - 4 years using the Czochralski technique. SBN is a solid solution between $SrNb_2O_6$ and $BaNb_2O_6$. Although the end members $SrNb_2O_6$ and $BaNb_2O_6$ do not belong to the tungsten bronze structural family, the solid solution $Sr_{1-x}Ba_xNb_2O_6$, $0.25 \leq x \leq 0.75$, crystallizes in the tetragonal tungsten bronze structure.[1] Figure 1 shows the limit of solid solution range for the three different phases, namely $SrNb_2O_6$, $BaNb_2O_6$ and tungsten bronze $Sr_{1-x}Ba_xNb_2O_6$, and the variation of the ferroelectric phase transition temperature for the bronze solid solution. Since this solid solution extends over a wide compositional range, bulk single crystal growth by the Czochralski technique becomes very difficult. The main problem associated with this technique can be summarized as the instability of the crystal diameter and thermal cracking. Inhomogeneity along the growth direction and core causes strain central to the growth axis, and accounts for the presence of striations in the crystals. The problem associated with coring has been eliminated in SBN:60 single crystals to a large extent by pulling the crystals at a composition as close to the congruent melt as possible. However, striations are still somewhat of a problem in the present crystals and they are

Table 1

Classification of Tungsten Bronze Family

T.B. Compositions with Smaller Unit Cell Dimensions e.g., $Sr_{1-x}Ba_xNb_2O_6$, $Sr_2KNb_5O_{15}$, $Sr_2NaNb_5O_{15}$	T.B. Compositions with Larger Unit Cell Dimensions e.g., $Ba_6Ti_2Nb_8O_{30}$, $Sr_2Ti_2Nb_8O_{30}$, $Ba_{2-x}Sr_xK_{1-y}Na_yNb_5O_{15}$, etc.
• Crystal Habit is Cylindrical with 24-Define Facets	• Crystal Habit Square with 4-Define Facets
• High Electro-Optic and Pyroelectric Effects	• High Electro-Optic Coefficient
• High Dielectric Constant	• Relatively Low Dielectric Constant
• High Piezoelectric d_{33} Coefficient but Low d_{15}	• High Piezoelectric d_{15} Coefficient but Moderate d_{33}
• Large Crystals with Excellent Quality Available (2 - 3.0 cm in Diameter)	• Moderately Large Crystals are Available (~ 1 - 1.5 cm)

believed to be associated with several experimental factors. Most authors concerned with the growth of SBN report the existence of striae (or refractive index variations) in these crystals. The striae are generally attributed to variations in the growth temperature causing variations in the composition, in particular the Sr/Ba ratio. Besides this problem, we suspect that there are some other problems which are responsible for introducing striations in SBN single crystals. They are as follows:

a. Reduction of Nb^{5+} to Nb^{4+} at the growth temperature (if oxygen pressure is low). Nb^{4+} acts as an impurity.

b. Presence of impurities e.g., Ca^{2+} and Fe^{3+}, in the starting materials. Initially reagent grade chemicals were used in this work.

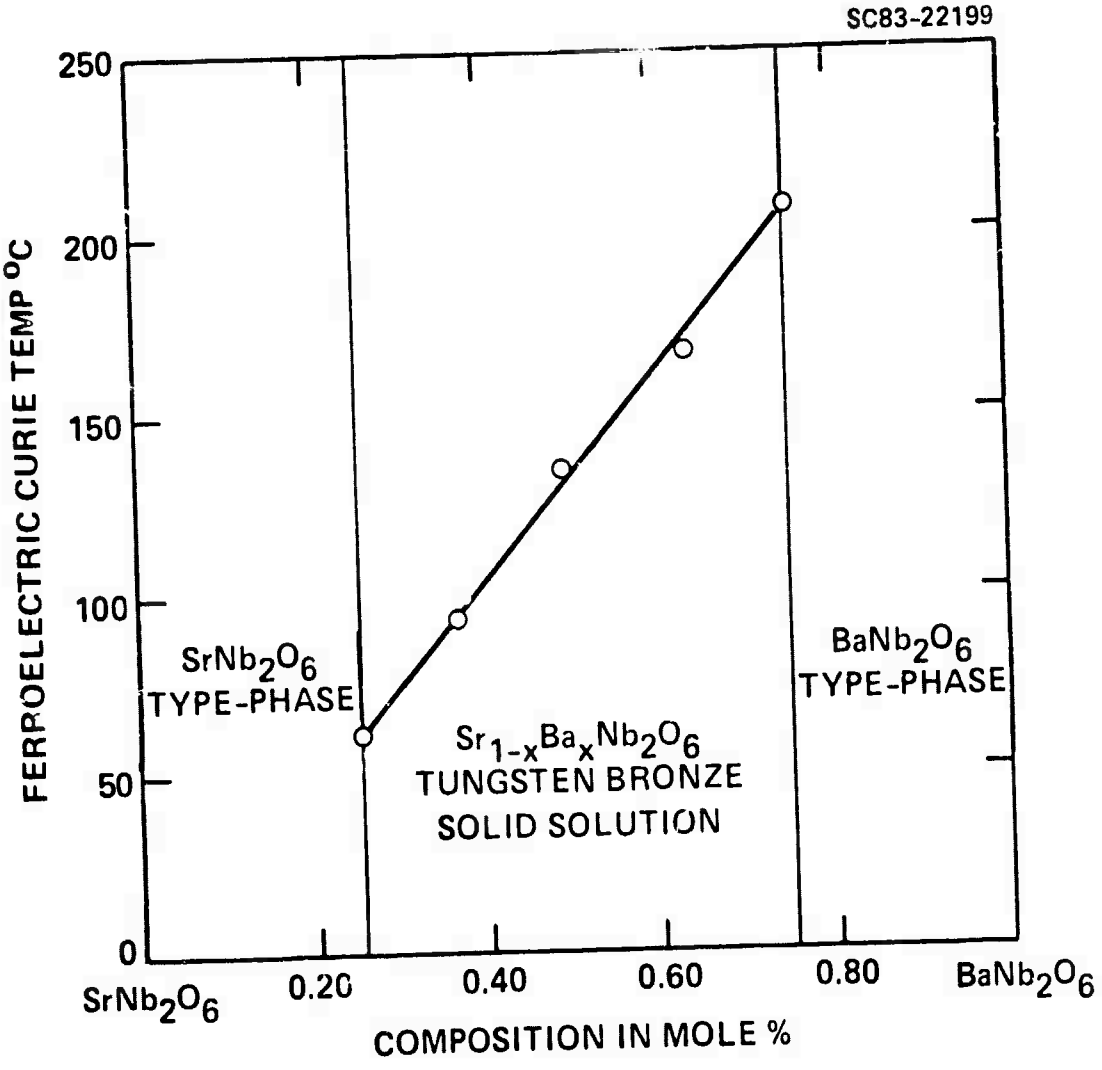

Fig. 1 Phase boundary and Curie temperature vs composition for $Sr_{1-x}Ba_xNb_2O_6$.

c. Temperature fluctuation in our old pulling unit (± 3- 5°C) responsible for excessive temperature instability.

d. Pulling and rotation rates are found to affect the presence of striations in the crystals.

2.4 Current Status of SBN:60 Crystals

Single crystal growth of SBN:60 has been modified in the present work in order to improve the crystal quality and thereby enhance its use for optical studies. Since the SBN:60 composition is reported to be the only congruent melting composition in the $SrNb_2O_6$-$BaNb_2O_6$ system,[2] the current effort has concentrated on this composition to develop optical quality crystals. As discussed in the preceding section, there are several factors which influence the quality of this crystal; hence it is important that the necessary modification be made in our growth procedure. The changes made are as follows:

a. Use of higher purity starting materials (refer to Table 2) to eliminate iron, calcium, magnesium, etc.

b. Eliminated the use of iridium crucible: no iridium contamination.

c. Large crucible and small crystals to minimize compositional gradients.

d. Installed a new Czochralski growth unit to minimize temperature instability.

The new crystal growth unit has been in service for the last six months and the system has been modified to provide further improvements in temperature stability (± 2°C). If it is necessary, other modifications will be made in this system to achieve even better temperature stability. The growth procedure and results are discussed in the following sections.

2.4.1 Growth Procedure

Nb_2O_5, $SrCO_3$ and $BaCO_3$ fine powders have been used as starting materials and weighed out in the desired proportions as summarized in Table 2. The batch mixture is ball-milled in acetone for 20 - 30 hr, and then poured into a large drying dish. The dric powder is placed in a platinum reaction dish and calcined at 1000°C for 10 - 15 hr to eliminate carbonates and any possible carbon from pyrolytic breakdown of residual acetone. The calcined powder is then ball-milled again and refired in an oxygen flow of 2 cfh at 1400°C for about 4 - 6 hr. A phase check and x-ray lattice constant measurements are made for each batch to ensure the use of a phase-pure bronze composition for crystal growth. A thick-walled platinum crucible of 2 × 2 in. in dimension is used for this growth, and this container holds roughly 450 grams of melt composition. A schematic of the Czochralski growth apparatus is shown in Fig. 2.

2.4.2 Growth Results

Table 3 gives a brief summary of our crystal growth efforts on SBN:60 and SBN:50 single crystals grown under different conditions. The SBN:60 single crystals have been pulled from both iridium and platinum crucibles with successful results. In the case of iridium crucibles, argon or nitrogen pressure had to be used to prevent oxidation and excessive loss of iridium, and as-grown crystals were found to be dark purple to coal black in color. However, the color changed to deep yellow, but not colorless, when the crystals were annealed in oxygen at greater than 1000°C. It seems that the coloration is related to the inclusion of iridium impurities; hence, the use of an iridium crucible for this growth has been curtailed. In the case of platinum crucibles, an oxygen atmosphere was used and the crystals thus obtained were colorless to pale yellow, depending on the diameter of the crytals and the oxygen pressure. Brice et al[3] studied the single crystal growth of the composition $Sr_{0.7}Ba_{0.3}Nb_2O_6$ and reported that the oxygen pressure should be over 2 atmosphere to produce colorless crystals. The results of this work are in agreement with these results only for small crystals, typically of approximately 1.5 cm diameter or

Table 2

Materials For Bulk Single Crystal Growth Work

	Purity and Mole% of Starting Material	Remarks*
Starting Materials	a. $SrCO_3$ - Johnson Mathey Chem. (99.999%)	* Fe^{3+}, Cu^{2+}, Ca^{2+} < 1.0 ppm
	b. $BaCO_3$ - Johnson Mathey Chem. (99.999%)	* Mg^{2+}, Na^{+}, In^{3+} ~ 1.0 ppm
	c. Nb_2O_5 - Automergic Chem. Met. (99.970%)	* No anionic impurities detected.
Batch Mixture SBN:60	a. $SrCO_3$ ----- 135.08 gms b. $BaCO_3$ ----- 115.45 gms c. Nb_2O_5 ----- 398.73 gms Total wt ----- 649.26 gms Total wt ----- 450.0 gms used for growth	* Congruent melting composition * Large crystal can be produced, approximately 1" in diameter. * Use as host crystal as well as substrate material for LPE work. * Exhibit high electro-optic and pyroelectric coefficients. * Melts ~ 1510°C and no spattering observed.
Batch Mixture SBN:50	a. $SrCO_3$ ----- 92.26 gms b. $BaCO_3$ ----- 123.34 gms c. Nb_2O_5 ----- 332.27 gms Total wt ----- 547.87 gms Total wt ----- 450.0 gms used for growth	* Slightly off congruent melting composition * Large crystals are available * Use as substrate material for LPE work. * Modified crystals exhibit excellent pyroelectric properties. * Melts ~ 1520°C

* Analysis was performed using optical emission Arc spectrography.

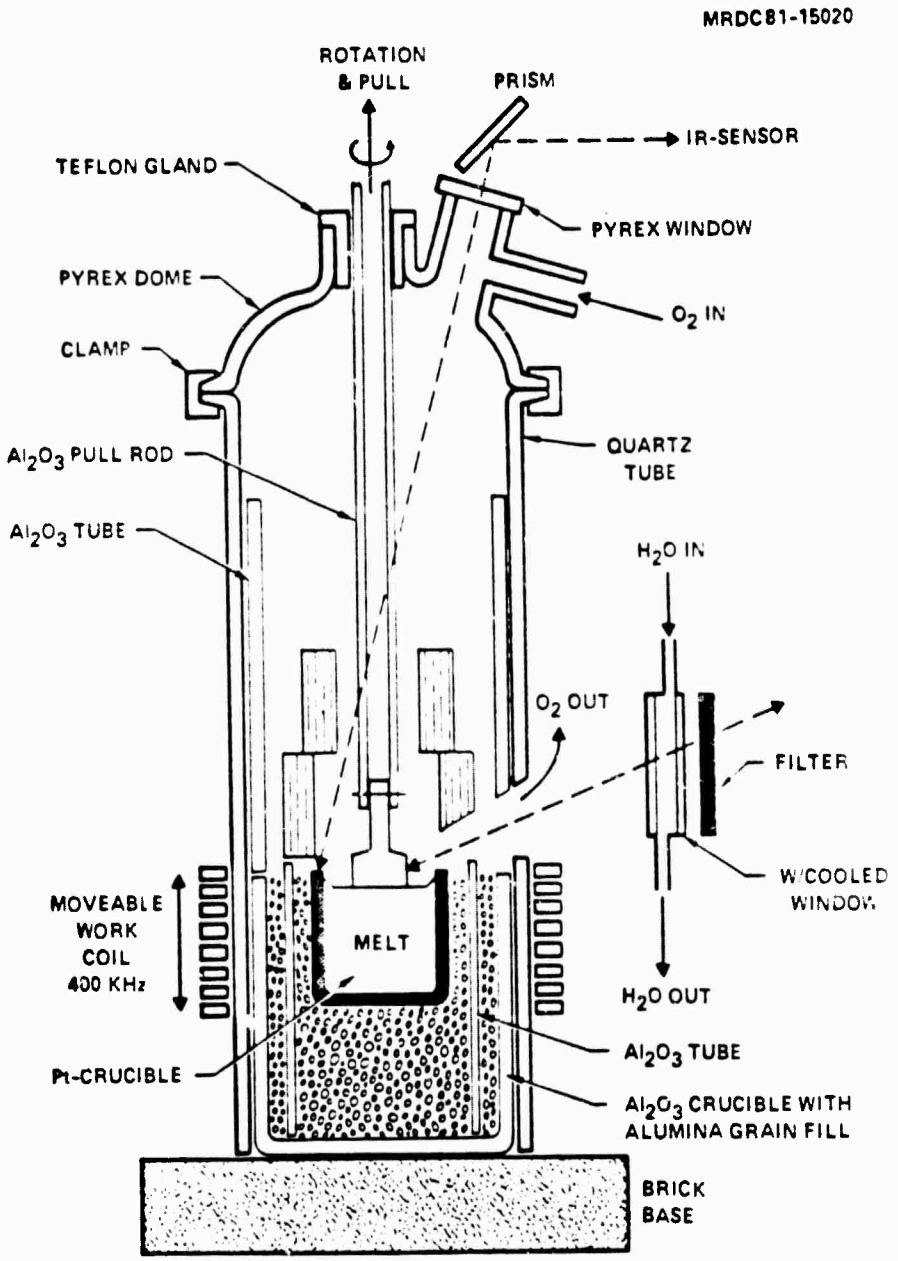

Fig. 2 A schematic diagram of a typical Czochralski crystal growth apparatus.

Table 3

Growth of SBN-Single Crystals

Exp No.	Composition	Growth Direction	Pull Rate	Rotation Rate (rpm)	Boule Weight (gms)	Growth Temperature (°C)	Color	Remarks
126	SBN:60	001	6 mm/hr	0 - 20	10	1510	Colorless	7 mm in diameter 3 cm long
127	SBN:60	001	5 - 6 mm/hr	0 - 10	58	1510	Pale Yellow	ADC - uncracked
133	SBN:60	001	5 - 6 mm/hr	5	20	1510	Pale Yellow	ADC - uncracked
134	SBN:60*	001	6 - 8 mm/hr	10	35	1510	Pale Yellow	ADC - uncracked
142	SBN:60	001	2 - 10 mm/hr	0 - 30	~ 10	1510	Almost Colorless	Uncracked
143	SBN:60	001	3 - 15 mm/hr	0 - 10	9	1510	Almost Colorless	Cracked on cutting
144	SBN:60*	001	8 - 12 mm/hr	5 - 8	21	1510	Pale Yellow	ADC - uncracked.
145	SBN:60	001	8 - 12 mm/hr	5 - 8	18	1510	Pale Yellow	ADC - uncracked
147	SBN:60	001	8 - 15 mm/hr	3 - 9	24	1510	Pale Yellow	Half crystal cracked
123	SBN:50	001	7 mm/hr	10	16	1520	Pale Yellow	Cracked on cutting
124	SBN:50	001	8 mm/hr	8	20	1520	Pale Yellow	Cracked severely
125	SBN:50	001	8 mm/hr	8	30	1520	Pale Yellow	Uncracked
132	SBN:50*	001	8 mm/hr	10	28	1520	Pale Yellow	Re-annealed at 1200°C, uncracked
146	SBN:50	001	6 mm/hr	5	27	1520	Pale Yellow	Re-annealed, uncracked

SBN:60 - $Sr_{0.6}Ba_{0.4}Nb_2O_6$, * - Samples sent to NRL.

SBN:50 - $Sr_{0.5}Ba_{0.5}Nb_2O_6$ ADC - Automatic diameter control.

smaller. Above this limit, the crystals appear to be pale yellow, and this color becomes deeper as the size of the crystal increases.

Fracture-free and reasonably good quality single crystals of approximately 1 - 3 cm in diameter have successfully been produced. Although the growth of 3 cm or bigger crystals is possible in the present set-up,[4] the technique at present is confined to smaller size crystals, typically 1 - 1.5 cm in diameter. Figures 3 and 4 show typical 1.5 cm diameter and 3 - 4 cm long SBN:60 and SBN:50 single crystals pulled along the c-axis. The crystals are pale yellow and those grown along the c-axis are usually well faceted, which is quite exceptional for Czochralski-grown crystals. X-ray diffraction studies show that the crystal habits are based on 24 faces of four prisms: (110), (120), (100) and (130). The observations are in excellent agreement with results reported by Dudnik et al[5] for SBN solid solution single crystals. The idealized form of the crystal is shown in Fig. 5.

The SBN single crystals have been evaluated by a variety of techniques to establish the crystal quality in terms of striations and other defects. Structural analysis by the x-ray diffraction technique for ceramic powders and single crystals of SBN:60 reveal that both the powder and crystal forms show a room temperature tetragonal tungsten bronze structure and, according to the structural refinements, possess 4 mm point symmetry. This is consistent with results reported for this solid solution by Jamieson et al.[6] The lattice constant measurements for the ceramic and single crystal samples of the SBN:60 composition give values of a = 12.464A and c = 3.941A, which are in close agreement with values 12.461A and 3.936A reported by Megumi et al.[2] These values are consistent from one crystal to another, indicating that the compositional variations are negligible as a result of the improved temperature stability during growth.

Since the Curie temperature of the bronze solid solution $Sr_{1-x}Ba_xNb_2O_6$, as shown in Fig. 1, is known to shift toward a higher temperature with increasing Ba^{2+} content,[1] each crystal was tested to evaluate its composition by establishing the Curie temperature. This has been accomplished by measuring the

SC83-22628

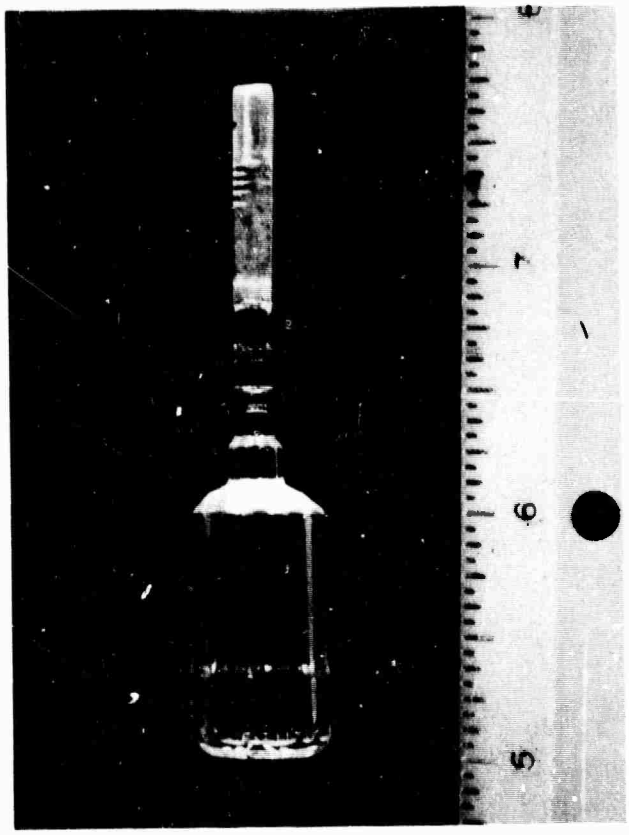

Fig. 3 SBN:60 single crystal grown along the (001) direction.

SC83-22629

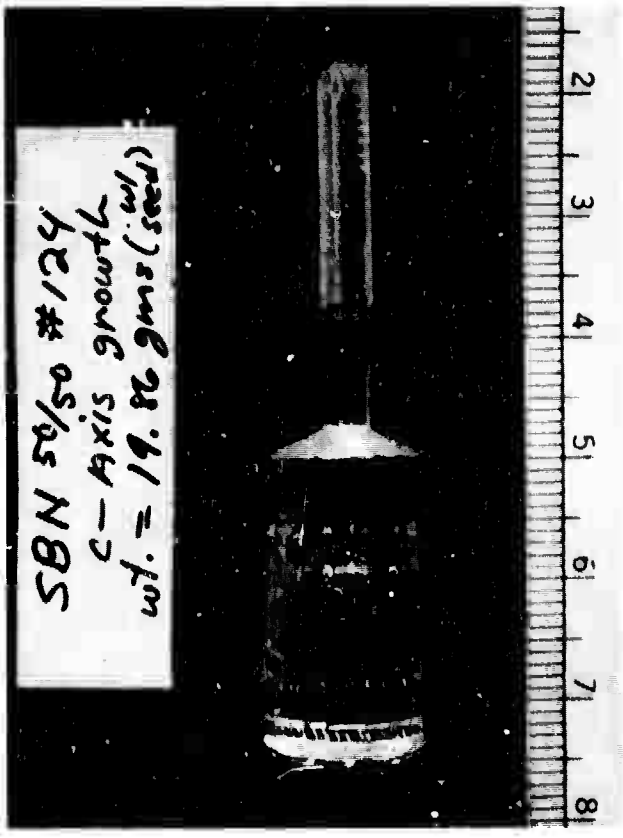

Fig. 4 SBN:50 single crystal grown along the (001) direction.

ERC80-9419

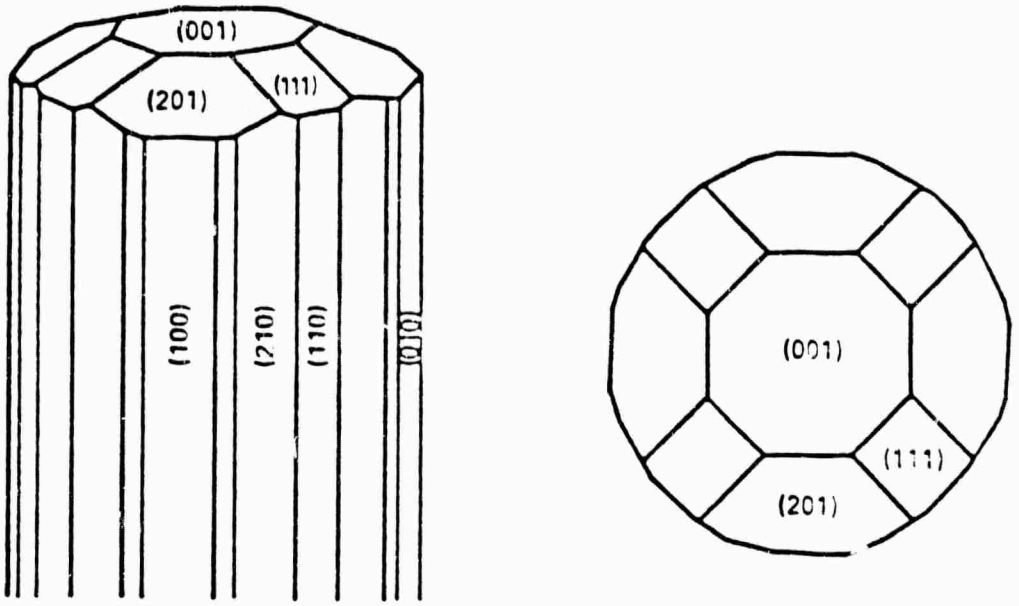

Fig. 5 Idealized form of SBN solid solution crystals.

temperature dependence of the low frequency permittivity over the temperature range of 20° to 140°C. The Curie temperature for all of the SBN:60 specimens, including ceramics and crystals (different parts and different crystals) occurred at 72 ± 1°C, which is again in excellent agreement with results reported by Magumi et al[2] for this composition. All of these tests strongly suggest that the crystal composition is homogeneous and that it is very close to the congruent melting region. It seems that the improved temperature stability in the new unit and the use of an automatic diameter control (ADC) system have played an important role in pulling better quality crystals, specifically in controlling the coring problem in both the SBN:60 and SBN:50 crystals. The use of the ADC system allowed us to pull a constant weight of SBN material per unit time. We believe that this has considerably minimized defects, including coring and compositional inhomogeneity. Although striations have been observed in SBN:60 crystals, the current results are considered to be a positive step forward in improving the material quality and physical properties.

Optical evaluation has also shown the existence of striations in SBN:50 crystals. Since SBN:50 is not a congruent melting composition, the Czochralski growth of striation-free crystals will be very difficult. These crystals will primarily be used as substrate material for the LPE growth work. Figure 6 shows the striation pattern (20 - 25 μm separation) observed for SBN:60 crystals, and they appear in the form of a perturbation of the refractive index parallel to the growth front. The existence of these striations has been studied in this work as a function of starting material purity (less Ca^{2+} and Fe^{3+}), crystal rotation during growth, and changes in the post-annealing treatment.

Recently we analyzed several crystals which were grown using analar grade as well as higher purity chemicals, and found that striations are definitely connected to a nonuniform distribution of impurity ions such as Ca^{2+}, Fe^{3+}, Nb^{4+}, and Ir^{4+} (if an Ir crucible is used). These impurities were found to be on the order of 80 ppm or higher in concentration (analar grade chemicals), and greatly affect crystal quality and coloration. For example, Fe^{3+}-containing crystals are deep yellow in color, while Nb^{4+}- and Ir^{4+}-containing

SC83-22630

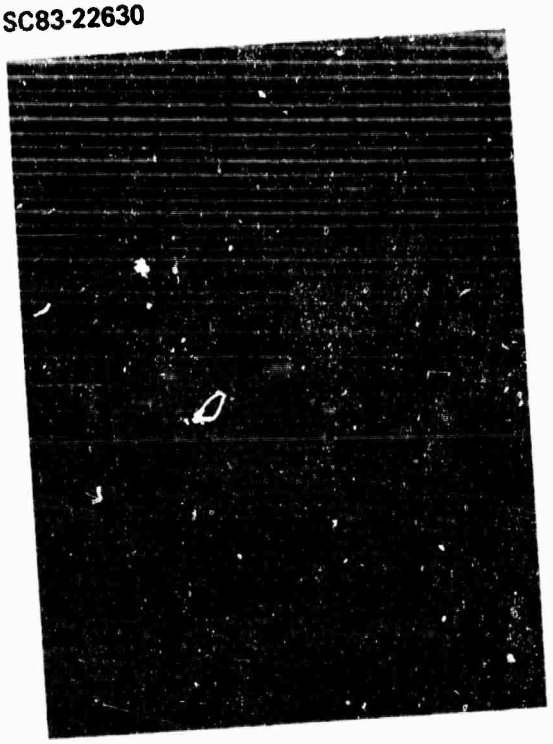

Fig. 6 Microphotograph by transmitted light showing striation pattern for SBN:60 crystal.

crystals were purple to coal black in color, depending on the concentration of impurity ions. The inclusion of Nb^{4+}, which results from a reduction of Nb^{5+}, has been eliminated to a large extent by employing an oxygen pressure of two atmospheres or more. Since the concentration of Fe^{3+} and Ca^{2+} is significantly lower in higher purity starting materials, striations are substantially reduced, but do not completely disappear. Based on these observations, it is clear that future experiments can be redesigned by either improving the temperature stability during growth and/or by use of still higher purity chemicals. At this stage, it appears that temperature stability is now a more significant factor and plans are underway to modify the thermal gradient in and above the crucible. We believe that if we can succeed in controlling temperature stability to 0.5 - 1.0°C or better, it may be possible to significantly reduce striations.

The effects of crystal rotation and pulling rates on striations have also been studied very carefully, and it has been shown that the pulling rate has no significant effect on crystal quality. However, the rotation rate seems to play a dominant role in crystal growth, and crystal sections were found to be free of striations when rotation was stopped or else kept at a higher speed, typically over 75 rpm. Although this is a very promising result, it was found very difficult to pull crystals under such conditions, especially when the rotation was completely stopped. It seems that pulling crystals at a somewhat lower rate and at zero rotation suppresses the striations which result from a radial dissymmetry of the thermal gradient around the pulling axis. Further efforts in this direction are underway, and if we succeed in designing a suitable arrangement for such growth, striations should not be a difficult problem.

Finally, we have also examined the effects of post-annealing on striations and the cracking of crystals grown using either higher purity or analar grade starting materials. This has been accomplished by holding the crystal just over the melt surface at 1100° - 1200°C for approximately 4 - 6 hr and then slowly cooling to room temperature. As shown in Fig. 7, striations in SBN:60 crystals grown from higher purity materials almost disappear under these annealing conditions, and the crystals are homogeneous and crack-free. On the other hand, crystals grown from analar grade materials still exhibit striations

SC83-22631

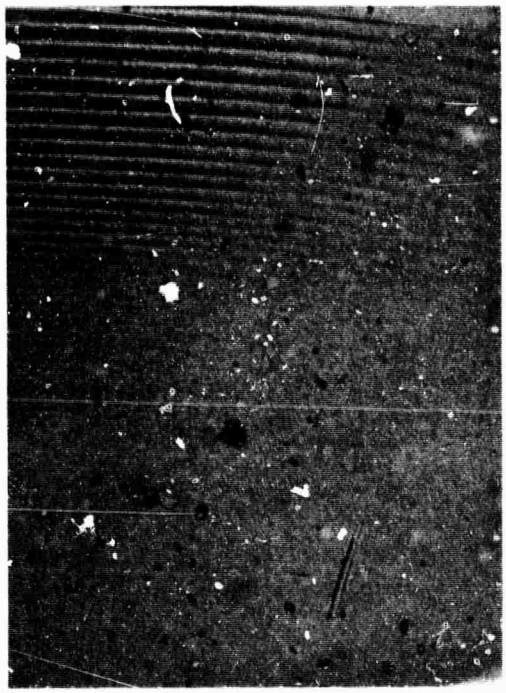

Fig. 7 Suppression of striations for SBN:60 crystals grown under improved temperature conditions.

even after annealing at higher temperatures, indicating that the striations introduced by impurity ions are difficult to remove. These results suggest that the striations developed in the first case seem to be associated with a change in the Sr/Ba ratio during growth and this change may be the result of temperature instability. Based on all of these observations, we expect that by improving the temperature stability further in our current growth and post-annealing conditions, it should be possible to minimize striations. During the next six months, the following changes will be tried to improve the current growth of SBN:60 crystals. They are as follows:

- Improve temperature stability to maintain a constant Sr/Ba ratio.
- Increase rotation rate to 75 - 100 rpm.
- Reduce Ca^{2+} and Fe^{3+} concentration in the melt.

3.0 LIQUID PHASE EPITAXIAL GROWTH OF BRONZE COMPOSITIONS

3.1 Introduction

The purpose of the liquid phase epitaxial (LPE) growth work is to develop optical quality, modified tungsten bronze compositions that possess high electro-optic coefficients with a moderately low dielectric constant. The ability of LPE to obtain a wide variety of films in a relatively short time, compared with the time required to achieve suitable quality single crystals, will enable us to greatly expand our knowledge of obtainable properties in this class of materials. Since large size single crystals of the bronze composition $Sr_{1-x}Ba_xNb_2O_6$, x = 0.40 and 0.50, are now available from our current work, and secondly, since LPE growth of $Sr_{0.5}Ba_{0.5}Nb_2O_6$ has been shown to be successful,[7] this approach seems to be very appropriate for this work. Bronze compositions based on the tetragonal solid solutions $Sr_{1-x}Ba_xNb_2O_6$, $Pb_{1-x}Ba_xNb_2O_6$, $Ba_{2-x}Sr_xK_{1-y}Na_yNb_5O_{15}$ and $Sr_2KNb_5O_{15}$ (SKN) exhibit excellent electro-optic characteristics and appear to be promising candidates for optical wave guide and modulator applications. The LPE growth of SBN bronze compositions has already been initiated and is briefly discussed in the present report. Table 4 summarizes the physical properties of the $Sr_{1-x}Ba_xNb_2O_6$ and $Sr_2KNb_5O_{15}$ compositions.

3.2 Growth Procedure

The apparatus for growing thin films of $Sr_{1-x}Ba_xNb_2O_6$ solid solutions by the liquid phase epitaxial growth technique is shown in Fig. 8. It consists of dipping a polished substrate into a solution which is supersaturated with respect to the compound to be grown.

In detail, the solution, contained in a platinum crucible, is maintained at a precisely controlled growth temperature (approximately 950° - 1000°C) after having been heated to a higher temperature (approximately 1200° - 1250°C) to effect complete solution. When equilibrium has been established, the substrate is slowly lowered into the furnace, held just above the surface of the

Table 4

Physical Properties of the $Sr_{1-x}Ba_xNb_2O_6$ and $Sr_2KNb_5O_{15}$ Compositions

Physical Constants	$Sr_{0.6}Ba_{0.4}Nb_2O_6$	$Sr_{0.5}Ba_{0.5}Nb_2O_6$	$Sr_2KNb_5O_{15}$
Structural Family	Tungsten Bronze	Tungsten Bronze	Tungsten Bronze
Symmetry	Tetragonal	Tetragonal	Tetragonal
Point Group	4 mm	4 mm	4 mm
Lattice Constants	a = 12.462Å c = 3.938Å	12.480Å 3.952Å	12.470Å 3.942Å
Curie Temperature °C	72	125	156
Dielectric Constant K_{33} at room temperature	880	500	1200
Electromechanical coupling coefficients	k_{33} = 0.47 k_{31} = 0.14 k_{15} = 0.24	k_{33} = 0.48 k_{31} = 0.137 k_{15} = ---	k_{33} = 0.44 k_{31} = --- k_{15} = 0.26

melt for a few minutes, and then slowly immersed in the solution. After the required time for film growth has elapsed the sample is then withdrawn from the melt.

3.3 Solvents for Tungsten Bronze SBN Compositions

Crucial to the success of isothermal LPE growth is the ability to supercool the solution without the occurrence of spontaneous nucleation. It is therefore necessary, before LPE growth can be performed, to find a suitable flux system (solvent) for each chosen bronze composition. As summarized in Table 5, there are a large number of solvents that have been identified for the SBN compositions; however, the choice in the present work is restricted to only the vandium-containing solvents. Based on our work on ferroelectric $LiNbO_3$ thin film growth[8-11] and the preliminary work on various bronze compositions, it has

MRDC81-15547

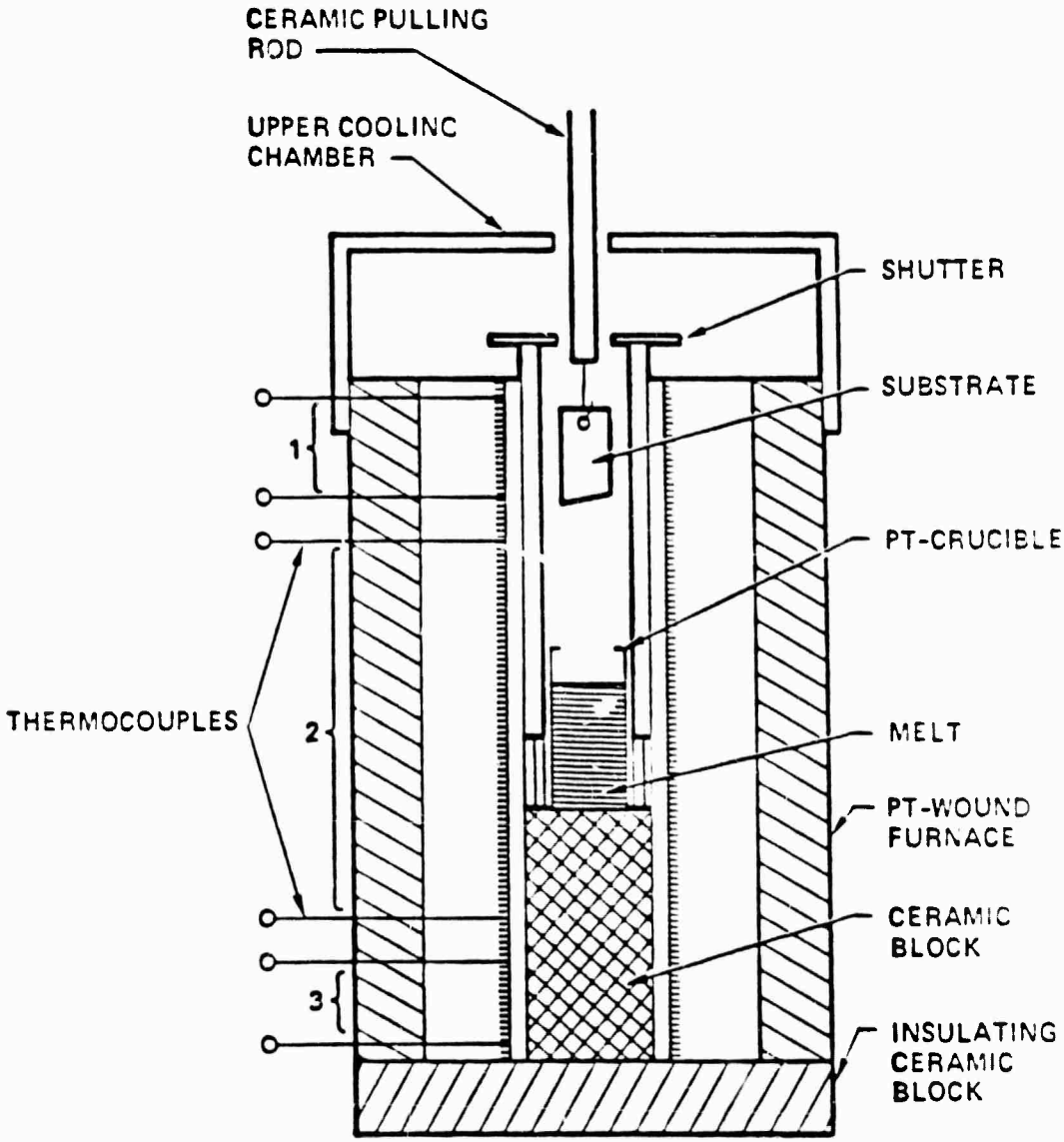

Fig. 8 LPE growth furnace.

Table 5

Solvents for the Tungsten Bronze Compounds

System	Flux Melting Temperature (°C)	Eutectic Temperature (°C)	Phases Present*	Remarks
BaV_2O_6-$Sr_{1-x}Ba_xNb_2O_6$	700	685	SBN	Long useful crystallization range
SrV_2O_6-$Sr_{1-x}Ba_xNb_2O_6$	750	--	SBN	Long useful crystallization range
KVO_3-$Sr_{1-x}Ba_xNb_2O_6$	520	490	SKN	Long useful crystallization range
$NaVO_3$-$Sr_{1-x}Ba_xNb_2O_6$	630	~ 560	SNN	Long useful crystallization range
V_2O_5-$Sr_{1-x}Ba_xNb_2O_6$	690	--	SBN + Unknown	Short-not suitable
$LiVO_3$-$Sr_{1-x}Ba_xNb_2O_6$	700	--	$LiNbO_3$ + Unknown	Not suitable

*1) SBN - $Sr_{1-x}Ba_xNb_2O_6$, tetragonal tungsten bronze structure.
2) SKN - $Sr_2KNb_5O_{15}$, tetragonal tungsten bronze structure.
3) SNN - $Sr_2NaNb_5O_{15}$, tetragonal tungsten bronze structure.

been found that the vanadium-containing solvents are preferable for SBN and other bronze compositions for the following reasons:

a. V^{5+} cation has a strong preference for the 4-fold coordinated site, and hence no vanadium inclusion in the bronze structure is expected.

b. Supercooling range for the V^{5+}-containing solvents is reasonably high, of the order of 20 to 40°C.

c. V^{5+}-containing solvents melt at significantly lower temperatures and thus allow LPE growth at much lower temperatures.

d. V^{5+}-containing solvents are remarkably stable at elevated temperatures.

e. All V^{5+}-containing solvents dissolve in water or dilute acids.

Since the tetragonal tungsten bronze structure extends over a wide compositional range in the $SrNb_2O_6$-$BaNb_2O_6$-BaV_2O_6 ternary system (Fig. 9), it is very important in this research to establish the Sr/Ba ratio for each composition crystallized in this system. This is a tedious and time consuming task; hence the work has to be confined to a small region of current interest at this time. Since SBN:50 single crystals exhibit a Curie temperature of around 120°C and lattice constants compatible with SBN:60 crystals, compositions in the BaV_2O_6-$Sr_{0.5}Ba_{0.5}Nb_2O_6$ system have been studied for LPE growth. The x-ray analysis of the BaV_2O_6-$Sr_{0.5}Ba_{0.5}Nb_2O_6$ system indicates that the tetragonal $Sr_{0.48}Ba_{0.52}Nb_2O_6$ composition crystallizes over a wide compositional region, and appears to be suitable for LPE growth. Table 6 summarizes the experimental data for this system, and based on these data it is clear that the lattice constant c varies somewhat with composition, but still the changes are too minor to shift the composition significantly.

The work on the BaV_2O_6-$Sr_{0.5}Ba_{0.5}Nb_2O_6$ system was continued to establish the composition-temperature relation using the differential thermal analysis (DTA) technique. Since the present system contains five or more components, the determination of a complete phase diagram in such a situation is impractical. Therefore, the system was treated as pseudo-binary. Figure 10 shows a composition-temperature relation diagram for the BaV_2O_6-$Sr_{0.5}Ba_{0.5}Nb_2O_6$ system. A pseudo-eutectic occurs at 15 mole% of SBN:50, above which $SrNb_2O_6$ ($0.15 < x < 0.35$) and $Sr_{0.48}Ba_{0.52}$-Nb_2O_6 phases were crystallized. The saturation temperature, i.e. the liquidus temperature for the bronze composition, is between 975° and 1500°C. The supercooling range for the system is approximately 20°C, which is shown to be advantageous for the growth of SBN:48 films.

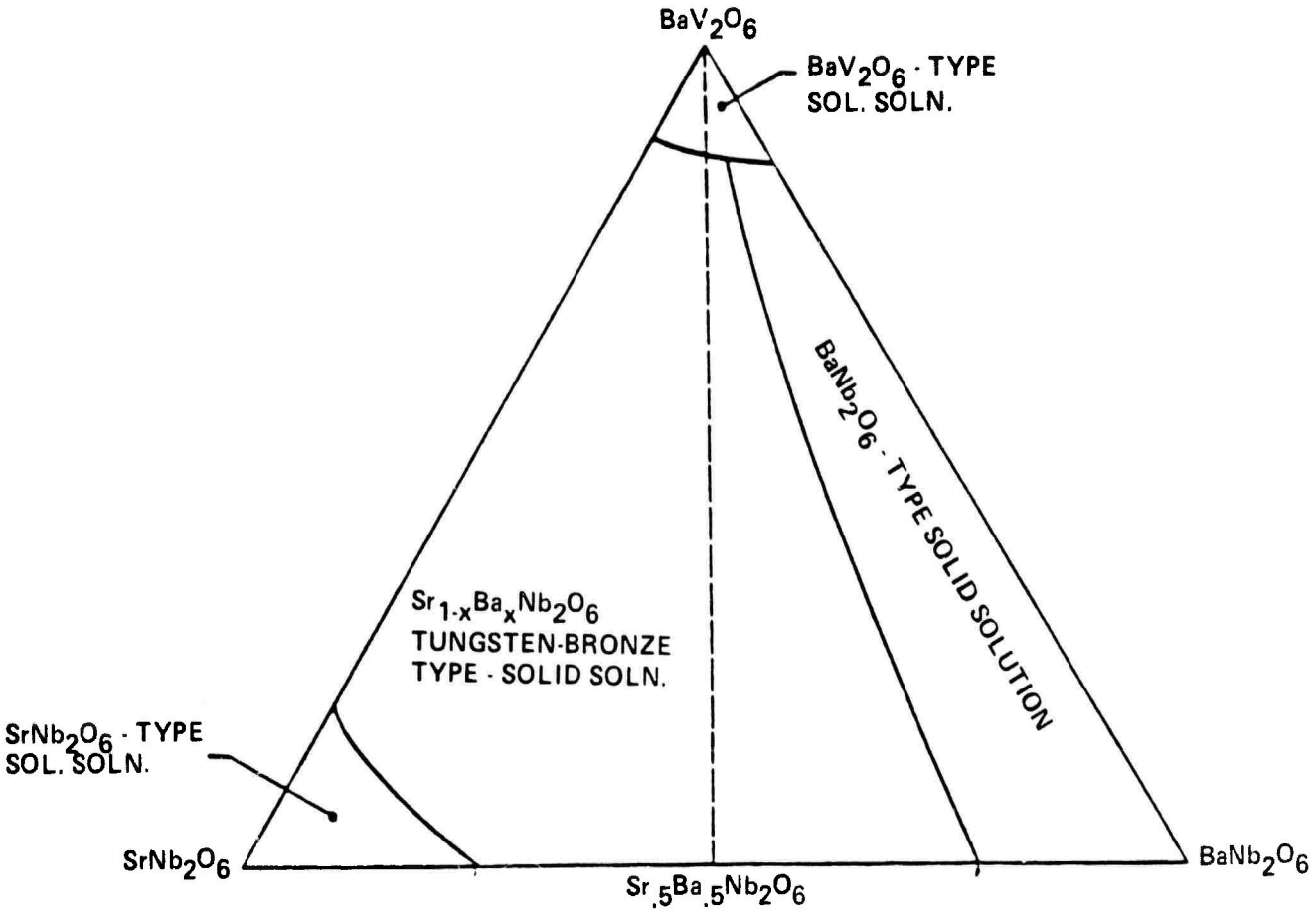

Fig. 9 The system $SrNb_2O_6$-$BaNb_2O_6$-BaV_2O_6, in air at 1200°C.

Table 6

Phase Analysis of the BaV_2O_6-$Sr_{0.5}Ba_{0.5}Nb_2O_6$ System

Composition*	Melting Temperature (°C)	Phases Identified	Lattice Constant (A) a	C
BaV_2O_6	720	BV	--	--
90% BV + 10% SBN:50	850	--	--	--
80% BV + 20% SBN:50	900	SN	--	--
70% BV + 30% SBN:50	955	SN + SBN	--	--
65% BV + 35% SBN:50	975	SBN:48	12.504	3.956
60% BV + 40% SBN:50	1050	SBN:48	12.504	3.958
50% BV + 50% SBN:50	1200	SBN:48	12.500	3.962
40% BV + 60% SBN:50	1300	SBN:48	12.500	3.965
SBN:50	1520	SBN:50		

* BV: BaV_2O_6
SN: $SrNb_2O_6$
SBN:48: $Sr_{0.48}Ba_{0.52}Nb_2O_6$
SBN:50: $Sr_{0.5}Ba_{0.5}Nb_2O_6$.

3.4 Epitaxial Growth of the Bronze SBN:48 Composition

The mixture containing 65 mole% BaV_2O_6 and 35 mole% $Sr_{0.5}Ba_{0.5}Nb_2O_6$ was selected, since this mixture melts at a relatively low temperature (975°C) and has been found to be suitable to develop thin films of the SBN:48 composition. For this growth, an approximately 100 cc platinum crucible was used with 400 grams of batch mixture. The weights of the individual chemicals in this mixture were as follows:

a. $BaCO_3$ = 162.80 gms
b. V_2O_5 = 118.30 gms
c. $SrCO_3$ = 25.83 gms
d. Nb_2O_5 = 93.10 gms.

MRDC79-7148A

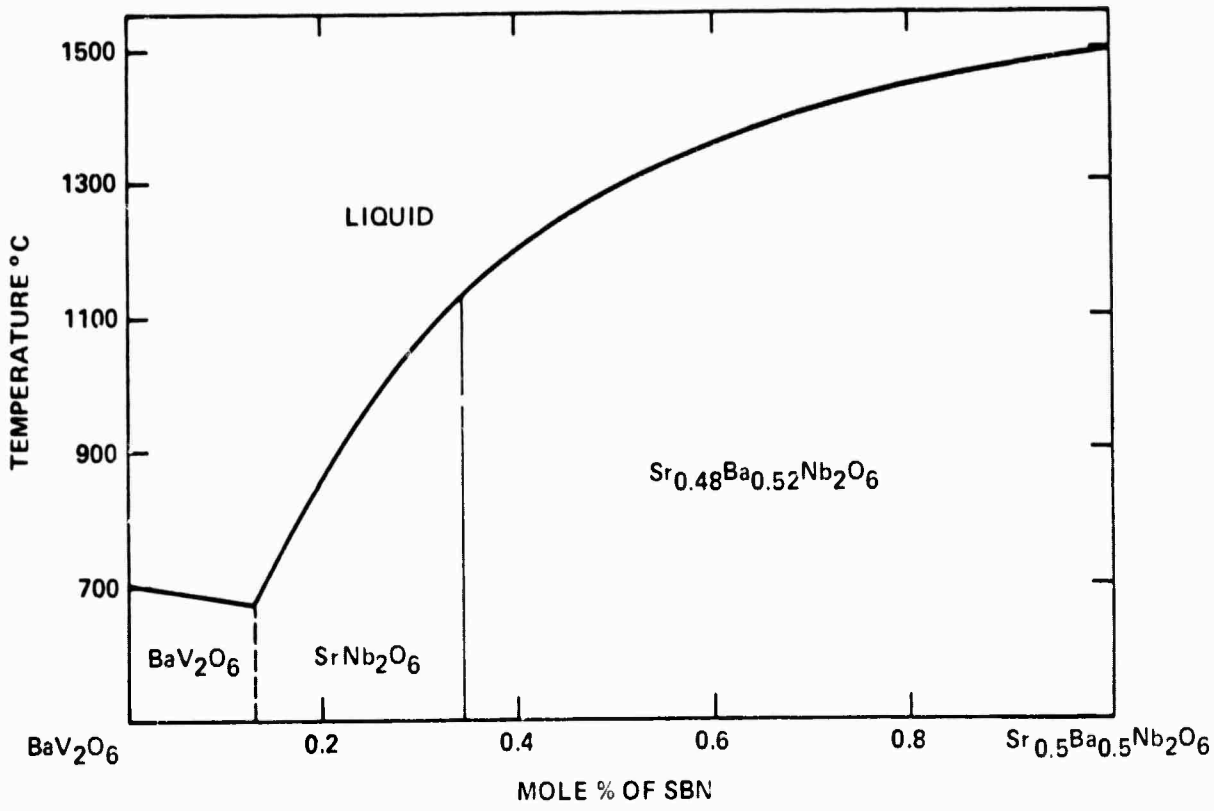

Fig. 10 Pseudo-binary phase diagram for BaV_2O_6-$Sr_{0.5}Ba_{0.5}Nb_2O_6$.

The batch was mixed in a large plastic bottle and then calcined at 650°C for about 15 hours prior to melting in the platinum crucible. The crucible was then placed in the growth furnace. As shown in Fig. 8, the growth apparatus consists of a vertical furnace which can be controlled with an accuracy of ± 1°C. The mixture was kept heated overnight at 1200°C and, after achieving complete homogeneity, the molten solution was slowly cooled to the growth temperature of around 1000°C at the rate of 10°C/hr. The (001), (100), or (110)-oriented SBN:60 substrate, positioned slightly above the melt in order to equilibriate with the solution temperature, was then dipped into melt. An appropriate dipping temperature was around 990° to 995°C. After the required time for growth elapsed, the sample was withdrawn from the melt and cooled very slowly to room temperature. The adhering flux was removed by dipping the substrate in dilute hydrochloric or nitric acid. Table 7 summarizes the results of these experiments.

These experiments have demonstrated the successful thin film growth of SBN:48 with films as thick as 15 - 20 μm. The results show that LPE growth is much faster on the (001)-plate compared to other orientations. This is consistent with our observations on bulk single crystal growth of SBN:60 and SBN:50 compositions, where growth is only possible along the (001) direction. The film growth on the other orientations is much slower; however, the surface of the films is much smoother due to a near-perfect lattice match. The films grown from the BaV_2O_6 flux are dark amber to yellow in color (due to the presence of V_2O_5), depending on the film thickness. Microscopic examinations at high magnification shows a slightly rougher aspect in the case of thicker films and films grown on the (001)-plate.

The crystallinity of the thin films has been established by x-ray diffraction measurements. A typical intensity vs epilayer thickness plot is given for the reflection (002) in Fig. 11. Two peaks corresponding to $CuK\alpha_1$ and $K\alpha_2$ represent the SBN:60 substrate, while the SBN:48 epilayer position is denoted by $CuK\alpha_1'$ and $K\alpha_2'$. The intensity of the epilayer reflection is significantly stronger than that of the substrate, indicating a high degree of crystallinity and successful growth of the SBN:48 layer on the SBN:60 substrate.

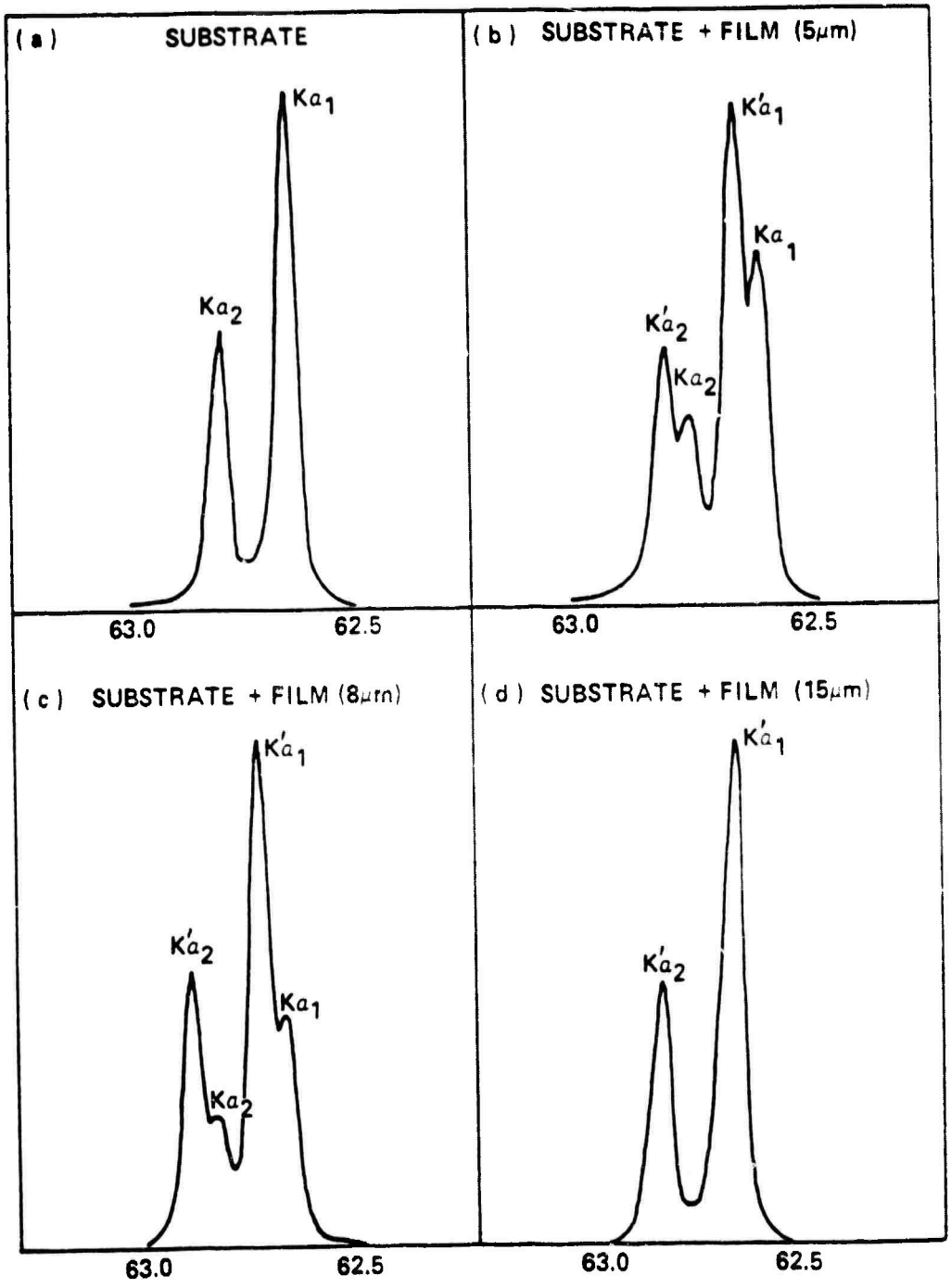

Fig. 11 X-ray diffraction peaks taken for substrate/film.

Table 7

Epitaxial Growth Conditions for the Bronze SBN:48 Composition

Composition	Substrate (Orientation)	Film Thickness (μm)	Quality	Remarks
65% BV + 35% SBN:48	SBN:60 (001)	10 - 15	Moderate	Slight mismatch
65% BV + 35% SBN:48	SBN:50 (001)	10 - 15	Good	Reduced mismatch
65% BV + 35% SBN:48	SBN:60 (100)	5 - 10	Excellent	Smooth Surface
65% BV + 35% SBN:48	SBN:60 (110)	5 - 10	Excellent	Smooth Surface

*Flux stays on substrate after growth; however, it can be washed away in dilute acids.

Recently Adachi et al[12] also demonstrated the successful growth of another bronze composition, $K_3Li_2Nb_5O_{15}$ (KLN), on bronze $K_2BiNb_5O_{15}$ substrates by both rf sputtering and LPE techniques. The $K_3Li_2Nb_5O_{15}$ films thus grown were shown to be of excellent quality with a thickness of approximately 3 - 4 μm. Although Adachi's work is similar to our present work, it appears that they were not successful in developing thicker films of $K_3Li_2Nb_5O_{15}$. Our current bulk crystal growth work on this bronze composition indicates that crystal growth of KLN is difficult due to a compositional shift during growth. Furthermore, this material does not possess a high electro-optic coefficient; hence this bronze composition has not been considered in the present study. Nevertheless, our current work opens new interest for this family and its application not only for electro-optic devices, but also in other areas such as spatial light modulators, pyroelectric, and surface acoustic wave devices.

3.5 Summary

Although we have successfully demonstrated the LPE growth of the SBN:48 bronze composition, still a number of questions need to be addressed before it can be used for device studies. They are as follows:

- Actual film composition.
- Surface finish necessary for device studies.

- How to pole films without depoling the substrate material.
- Film thickness necessary for the given device study.

During the next six months, plans are made to study some of these problems to decide the applicability of these films for device studies. We believe that poling of the films will be a critical task in future work and will need full attention to study this aspect. Although the film surfaces appear to be smooth, we expect that these surfaces will have to be tested with respect to the given device application. At present, films grown on (001)-plates are slightly rougher due to lattice mismatching, and hence this problem has to be studied in more detail using current substrates or other bronze crystals. The bronze SBN:50 (under DARPA contract) and BSKNN (under NVL and ONR contracts) crystals are being grown, and as soon as suitable size crystals become available, we expect that we will have a selection of substrate materials for the LPE work. This will speed up our work and should make it possible to develop suitable and different films for electro-optic applications.

4.0 THEORETICAL MODELING AND OPTICAL EVALUATION

4.1 Introduction

The goal of this investigation has been to assemble required dielectric and optical data for a selected range of ferroelectric tungsten bronze compositions so as to be able to define the quadratic prototypic electro-optic constants and the manner in which they mutate with compositions.

4.2 Theoretical Modeling

In the analysis of simple proper ferroelectrics like the bronze family, it is assumed that in the ferroelectric states P_s is the order parameter and that ancilliary changes which occur at the Curie temperature are essentially consequences of the appearance of a non-zero P_s value.

For a polarization vector appearing in the prototypic 4/mm symmetry the consequences upon the optical impermeability B_{ij} may be determined from the symmetry limited quadratic electro-optic coefficients which are, in this point group,

$$g_{11},\ g_{12},\ g_{31},\ g_{33},\ g_{44} \text{ and } g_{66} \ .$$

Thus the changes in the B_{ij}, i.e., ΔB_{ij}, may be written in the form

$$\begin{aligned}
\Delta B_{11} &= g_{11}P_1^2 + g_{12}P_2^2 + g_{13}P_3^2 \\
\Delta B_{22} &= g_{12}P_1^2 + g_{11}P_2^2 + g_{13}P_3^2 \\
\Delta B_{33} &= g_{31}P_1^2 + g_{31}P_2^2 + g_{33}P_3^2 \\
\Delta B_{23} &= g_{44}P_2P_3 \\
\Delta B_{13} &= g_{44}P_1P_3 \\
\Delta B_{12} &= g_{66}P_1P_2 \ .
\end{aligned} \tag{1}$$

For the tetragonal ferroelectric species 4/mm (1) D4F 4 mm in the notation of Shuvalov,[13] the matrix of ΔB coefficients reduces to

$$\Delta B_{11} = B_{22} = g_{13}P_3^2$$
$$\Delta B_{33} = g_{33}P_3^2 \qquad (2)$$

As would be expected, the optical properties retain the uniaxial character of the tetragonal symmetry (the loss of the mirror orthogonal to 4 does not change the optical character) and the only consequences of the phase change at T_c is a change in the standing birefringence Δn_{31}.

With the non zero value of P_3, however, P_{s3} in the ferroelectric states now gives rise to morphic linear electro-optic effects given by

$$\frac{\partial \Delta B_{11}}{P_3} = 2g_{13}P_{s3} = f_{13}$$
$$\frac{\partial \Delta B_{22}}{P_3} = 2g_{13}P_{s3} = f_{23}$$
$$\frac{\partial \Delta B_{33}}{P_3} = 2g_{33}P_{s3} = f_{23}$$
$$\frac{\partial \Delta B_{23}}{P_2} = g_{44}P_{s3} = f_{24}$$
$$\frac{\partial \Delta B_{13}}{P_1} = g_{33}P_{s3} = f_{15} \qquad (3)$$

where the f_{ij} are linear coefficients in polarization notation. The f are related to the more conventional r coefficients by

$$r_{13} = f_{13}\epsilon_{33} = 2g_{13}P_3\epsilon_{33}$$
$$r_{33} = f_{33}\epsilon_3 = 2g_{33}P_3\epsilon_{33}$$
$$r_{24} = r_{15} = f_{24}\epsilon_{11} = g_{44}P_3\epsilon_{11} \qquad (4)$$

where ϵ_{ij} is the dielectric permittivity.

From the polarization potential theory of DiDomenico and Wemple,[16] the g coefficient depends primarily upon the oxygen framework and should not change markedly with cation makeup, although in the lead containing compositions some systematic shifts may be expected. The morphic r coefficient, on the other hand, reflects strongly the behavior of P_s and of ε, which may be critically tuned by changing the Curie points θ_1 and θ_3 with cation substitution.

The temperature dependence of P_i and ε_{ij} can be effectively modeled using the modified Devonshire method[15] and this method has been demonstrated to be most effective in the SBN ($Sr_{1-x}Ba_xNb_2O_6$) bronzes.[16,17] With a family of g coefficients known, and the other thermodynamic parameters established for the non-linear polarizabilities, it should become possible to predict electro-optic behavior across the whole bronze family and eventually help in the search for compositions most suitable for various optical device applications.

4.3 Evaluation of Electro-Optic Coefficients

Magnitudes of the electro-optic g coefficients can be determined most easily from measurements of the birefringence Δn. For tetragonal symmetry, the birefringence is Δn_{31}, being the difference in the refractive indices n_3 and n_1. From Eq. (2) it can be easily shown that

$$\Delta n_{31} = \frac{1}{2} n_0^3 (\Delta B_{33} - \Delta B_{11}) \quad , \tag{5}$$

where n_0 is the refractive index of the unpolarized crystal. Therefore, we have

$$\Delta n_{31} = \frac{1}{2} n_0^3 (g_{33} - g_{13}) P_3^2 \quad . \tag{6}$$

Thus, if the values of P_3 and n_0 are known, the magnitude of the quantity $(g_{33} - g_{13})$ can be determined. Interestingly, this quantity is approximately equivalent to the electro-optic coefficient g_{44}, as reported by DiDomenico and Wemple.[14]

From these quantities and the appropriate dielectric constants, the electro-optic quantities ($r_{33} - r_{13}$) and r_{15} can then be determined using Eq. (4).

4.4 Experimental Procedure and Results

Ferroelectric tungsten bronze single crystals having the following compositions were selected for this investigation:

1. $Sr_{0.6}Ba_{0.4}Nb_2O_6$ - SBN (60:40)

2. $Pb_{0.56}Ba_{0.43}Nb_{2.006}O_6$ - PBN (60:40)

3. $Pb_{0.3}Ba_{0.7}Nb_2O_6$ - PBN (30:70)

All of the above compositions belong to the tetragonal point group 4 mm.

From the above bulk crystals, "a" cut plates were prepared into wedge shapes with a known angle (typically 7°). Using a polarizing microscope in conjunction with a hot stage, the birefringence Δn_{31} was determined as a function of temperature. A sodium lamp was used for the source of monochromatic light. The birefringence was calculated from the following equation:

$$\Delta n_{31} = \frac{\lambda}{d \sin \theta} \tag{7}$$

where λ is the wavelength of sodium light (5893A), d the width of interference fringes resulting from the varying thickness of the wedge, and θ the angle of the wedge.

The birefringence values as a function of temperature for the three crystal compositions are shown in Fig. 12. It is interesting to note that for all cases Δn_{31} passes through zero above T_c with a corresponding change in slope.

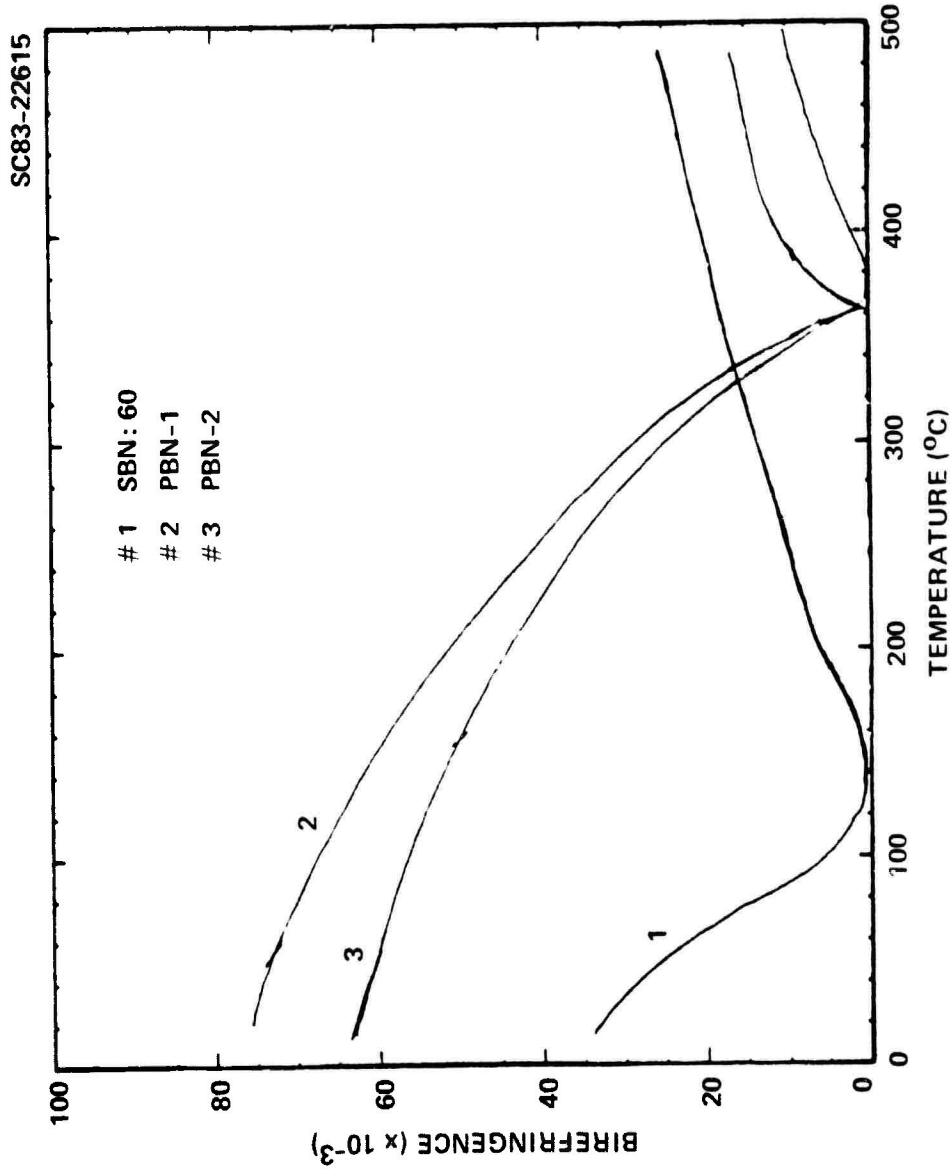

Fig. 12 Birefringence Δn_{31} vs temperature for PBN and SBN.

The birefringence measured below T_c, as shown in Fig. 12, is actually the sum of the polarization-induced birefringence (Eq. 2) and the temperature-dependent structural contributions $\Delta n_0(T)$ from the high-temperature phase (above T_c), i.e.,

$$\Delta n_{31}{}_{\text{measured}} = \frac{1}{2} n_0^3 (g_{33} - g_{13}) P_3^2 + \Delta n_0(T) \quad . \tag{8}$$

Using the approximated value of 2.3 for n_0 for all the crystals, and reported and calculated P_3 values, we obtained from Eq. (8) the quantity $(g_{33} - g_{13})$ and thus the approximate value of g_{44}. The values determined for all three compositions are reported in Table 8. Included in Table 8 are various dielectric constants which from Eq. (4) enable the calculation of the $(r_{33} - r_{13})$ and r_{15} quantities. For comparison, dielectric, piezoelectric and electro-optical data for other tungsten bronzes are also reported.

Knowing the change in P_s with temperature, as determined from pyroelectric data,[17-20] the temperature dependence of the quantity $(g_{33} - g_{13})$ could also be determined. Figure 13 shows the temperature dependence of $(g_{33} - g_{13})$ for the bronze compositions.

4.5 Discussion of Results

As can be seen in Table 8, the electro-optic quantities $(g_{33} - g_{13})$ and g_{44}, measured for the bronze compositions used in this investigation, were all found to be similar to one another and to those reported for other bronzes. As previously mentioned, this is in agreement with the theory of DiDomenico and Wemple[14] in which the g coefficients depend primarily upon the oxygen framework and should not change markedly with cation make up. The electro-optic g coefficients were also found to be virtually temperature independent, as shown in Fig. 13. Experimental error in the determination of Δn as f(T) could easily account for the slight temperature dependence shown.

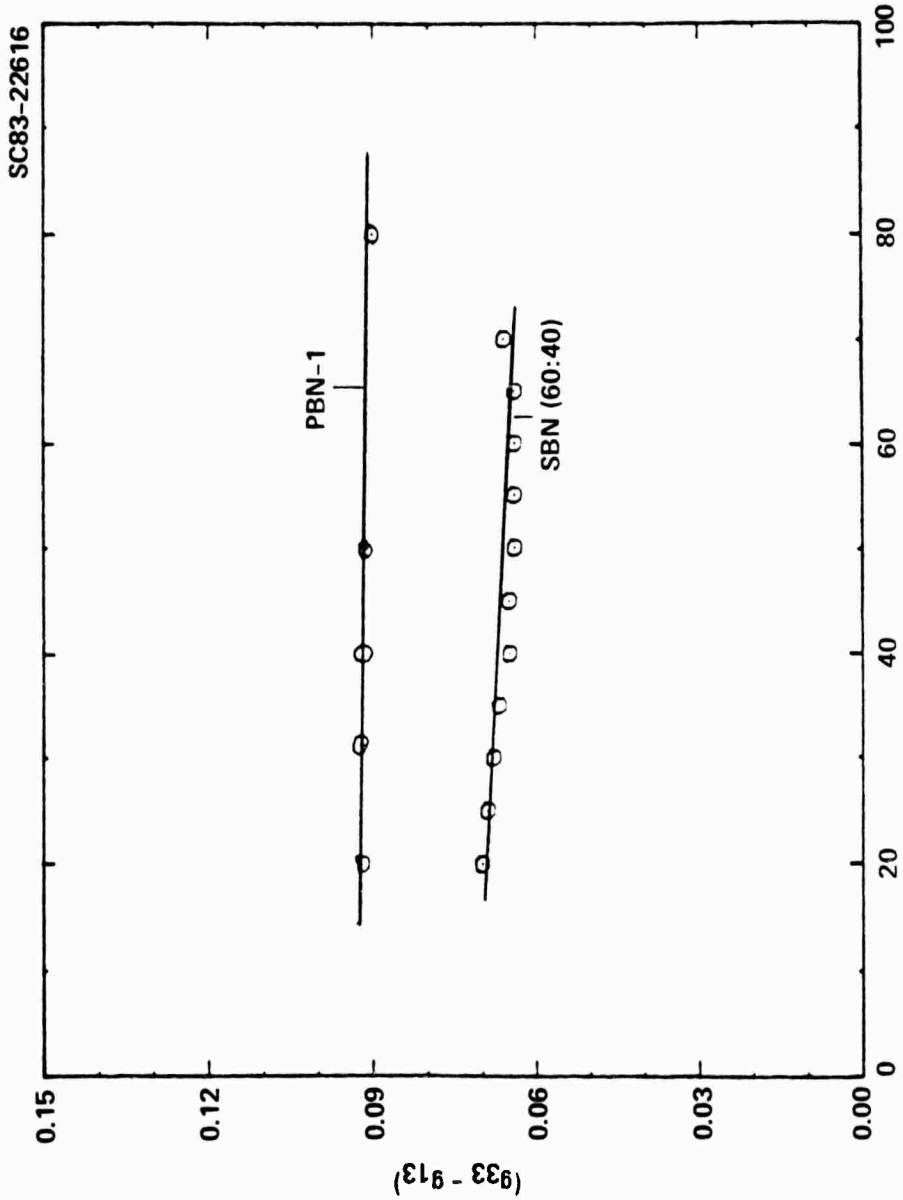

Fig. 13 Electro-optic quantity ($g_{33} - g_{13}$) vs temperature for PBN and SBN.

Table 8

Dielectric, Piezoelectric and Optical Data for Various Tungsten Bronze Crystals

Composition	T_c	Dielectric Permittivity		Piezoelectric Coefficient ($\times 10^{-12}$ C/N)			P_s (C/m^2)	Birefringence		Electro-Optic Coefficients: Quadratic (m^4/C^2)		Electro-Optic Coefficients: Linear (10^{-12} mV^{-1})	
		ϵ_{11}	ϵ_{33}	d_{31}	d_{33}	d_{15}		Δn_{meas}	Δn_{corr}	$g_{33}-g_{13}$	g_{44}	$r_{33}-r_{13}$	r_{15}
SBN (60:40)	72°C	470	880	-30	130	31	0.28	0.032	0.033	0.068	~ 0.068	300	~ 80
PBN-1	350°C	360	140	-12	60	50	0.40	0.078	0.092	0.094	~ 0.094	90	~ 120
PBN-2	345°C	1600	200		110	250	0.40	0.062	0.076	0.078	~ 0.078	110	~ 450
BNN[a]	560°C	242	51	-7	37	42	0.40			0.11	0.11	39	92
KLN[a]	405°C	306	115	-14	57	68	0.25			0.13		66	
BTN[a]	245°C	193	209				0.22			0.092		75	
SBN[a] (75:25)	56°C		6500				0.19			0.06		1300	42
SBN[a] (50:50)	118°C		500		90		0.29			0.09		220	

[a]Reported data for various tungsten bronzes.

BNN-$Ba_2NaNb_5O_{15}$, KLN-$K_{2.89}Li_{1.55}Nb_{5.11}O_{15}$, BTN-$Ba_3Nb_4TiO_{15}$,

SBN (75:25)-$Sr_{0.75}Ba_{0.25}Nb_2O_6$, SBN (50:50)-$Sr_{0.50}Ba_{0.50}Nb_2O_6$.

The electro-optic r coefficients, on the other hand, strongly reflect the temperature behavior of P_s and the dielectric constants similar to that of the piezoelectric d_{ij} coefficients given in Table 8. These properties can be critically tuned by changing the Curie temperatures θ_1 and θ_3. It should be noted that θ_3 is nearly equal to T_c. This is clearly shown by looking at the dielectric constant ε_{33}, d_{33}, and the quantity $(r_{33} - r_{13})$ of the various bronzes as a function of T_c, that is, the lower T_c the greater the values. Further evidence of this "tuning" is apparent from the differences in the ε_{11}, d_{15} and r_{15} coefficients between the two PBN compositions which have similar T_c's, but large differences in θ_1's.

The PBN (60:40) composition, being close to the tetragonal:orthorhombic morphotropic phase boundary,[20] greatly raises the transverse Curie temperature θ_1 from ~ 120°C for PBN (30:70) to ~ 240°C, effectively softening the transverse dielectric stiffness, resulting in exceedingly large k_{11}, d_{15} and r_{15} coefficients.

4.6 Summary

1. It has been shown that for the case of tetragonal ferroelectric tungsten bronzes, electro-optic g quantities can be easily obtained by measurement of the birefringence Δn_{31}.

2. The observed behavior of the g quantities was found to be consistent with other higher order coefficients, being only weakly composition and temperature dependent. However, additional measurements of the exact refractive indices, P_s, etc., are still needed.

3. It was also found that the electro-optic r coefficients behave similarly to the piezoelectric coefficients, being strongly affected by the behavior of P_s and ε, which may be tuned by changing the Curie points θ_1 and θ_3. The calculated quantities of $(r_{33} - r_{13})$ and r_{15} appear to be quite promising, particularly in the case of the PBN system. However, direct measurements of the r coefficients are still needed to check the calculated values.

4. With the family of g coefficients known, and the thermodynamic parameters established for the non-linear polarizabilities, it appears possible to be able to predict the pyroelectric, dielectric, piezoelectric, elastic, linear electro-optic and quadratic electro-optic behavior across the whole bronze family, and thus theoretically predict those compositions which will optimize combinations of property parameters required in the figure of merit for both electro-optic and acousto-optic applications.

5.0 FUTURE PLANNED WORK

- Improve the temperature stability and post-annealing conditions in the Czochralski growth unit developed for the bronze SBN:60 composition to produce minimum striation crystals.

- Improve the current Czochralski growth technique to develop approximately 2 to 2.5 cm in diameter SBN:50 composition single crystals. These crystals will be used as substrate material.

- Improve the LPE growth technique to develop thicker films, approximately 25 - 30 μm. Also establish the composition of the epilayers with respect to growth conditions.

- Establish the poling technique for epifilms and evaluate the ferroelectric properties, including dielectric, electro-mechanical, Curie temperature, piezoelectric and elastic.

- Identify suitable solvents for other important bronze compositions, e.g., $Sr_2KNb_5O_{15}$ and $Pb_{1-x}Ba_xNb_2O_6$.

- Establish more precise values for refractive indices, polarization, etc., with respect to temperature.

- Establish r coefficients (electro-optic) and compare with predicted values.

6.0 PUBLICATIONS AND PRESENTATIONS

6.1 Publications

1. T.R. Shrout, L.E. Cross and D.A. Hukin, "Ferroelectric Properties of Tungsten Bronze Lead Barium Niobate (PBN) Single Crystals," to be published in Ferroelectrics.

2. R.R. Neurgaonkar, W.K. Cory and J.R. Oliver, "Growth and Applications of Tungsten Bronze Family Crystals," to be published in Ferroelectrics.

6.2 Presentations

1. R.R. Neurgaonkar, W.K. Cory, and J.R. Oliver, "Growth and Applications of Tungsten Bronze Family Crystals," to be presented at the 1983 IEEE International Symposium on Applications of Ferroelectrics, June 1-3, 1983, Gaithersburg, Maryland.

7.0 REFERENCES

1. A.A. Ballman and H. Brown, J. Cryst. Growth 1, 311, (1967).

2. K. Megumi, N. Nagatsuma, Y. Kashiwada and Y. Furuhata, J. Mat. Sci. 11, 1583 (1976).

3. J.C. Brice, O.F. Hill, P.A.C. Whiffin and J.A. Wilkinson, J. Cryst. Growth 10, 133 (1971).

4. R.R. Neurgaonkar, M.H. Kalisher, T.C. Lim, E.J. Staples and K.L. Keester, M. Res. Bull. 15, 1235 (1980).

5. O.F. Dudnik, A.K. Gromov, V.B. Kravchenko, Y.L. Kopylov and G.F. Kunznetsov, Sov. Phys. Crystograph 15, 330 (1970).

6. P.B. Jamieson, S.C. Abrahams and J.L. Bernstein, J. Chem. Phys. 48, 5048 (1968).

7. R.R. Neurgaonkar, DARPA Final Report, Contact No. F49620-78-C-0093 (1982).

8. E.J. Staples, R.R. Neurgaonkar and T.C. Lim, Appl. Phys., Lett. 32, 197 (1978).

9. R.R. Neurgaonkar, M.H. Kalisher, E.J. Staples, and T.C. Lim, Appl. Phys. Lett. 35, 606 (1979).

10. R.R. Neurgaonkar, T.C. Lim, E.J. Staples, and L.E. Cross, Ferroelectrics 27, 62 (1980).

11. R.R. Neurgaonkar and E.J. Staples, J. Crystal Growth 54, 572 (1971).

12. M. Adachi, T. Shiosaki and K. Kawabata, Ferroelectrics 27, 89 (1980).

13. L.A. Shuvalov, J. Phys. Soc. Jpn. 28, 38 (1970).

14. M. DiDomenico, Jr., and S.H Wemple, J. Appl. Phys. 40, 720 (1969).

15. A.F. Devonshire, Phil. Mag. 40, 1040 (1949); Phil. Mag. 42, 1065 (1951).

16. T.R. Shrout (private communication).

17. T.R. Shrout, Ph.D. Thesis, The Pennsylvania State University (1981).

18. C. Huanchu, S. Yuhuan, and L.E. Cross, to be published in Mat. Res. Bull.